Nanoscale Res Lett (2007) 2:135–143
DOI 10.1007/s11671-007-9044-x

NANO EXPRESS

Combing and self-assembly phenomena in dry films of Taxol-stabilized microtubules

Fabrice Olivier Morin · Franck Rose · Pascal Martin · Mehmet C. Tarhan · Hideki Kawakatsu · Hiroyuki Fujita

Published online: 13 March 2007

Abstract Microtubules are filamentous proteins that act as a substrate for the translocation of motor proteins. As such, they may be envisioned as a scaffold for the self-assembly of functional materials and devices. Physisorption, self-assembly and combing are here investigated as a potential prelude to microtubule-templated self-assembly. Dense films of self-assembled microtubules were successfully produced, as well as patterns of both dendritic and non-dendritic bundles of microtubules. They are presented in the present paper and the mechanism of their formation is discussed.

Keywords Adsorption · HOPG · Microtubules · Self-assembly

Electronic Supplementary Material The online version of this article (doi:10.1007/s11671-007-9044-x) contains supplementary material, which is available to authorized users.

F. O. Morin (✉) · H. Kawakatsu · H. Fujita
LIMMS-CNRS/IIS, UMI 2820, University of Tokyo,
4-6-1 Komaba, Tokyo 153-8505, Japan
e-mail: morin@iis.u-tokyo.ac.jp

F. Rose
Materials Sciences Division, L. Berkeley National Laboratory,
One Cyclotron Road - Mailstop 66RO200, Building 66, Office
212, Lab 210, Berkeley, CA 94720, USA

P. Martin
L2MP, Institut Supérieur d'Electronique et du Numérique
Maison des Technologies, Pl. G. Pompidou, Toulon 83000,
France

M. C. Tarhan
IIS, University of Tokyo, 4-6-1 Komaba, Tokyo 153-8505, Japan

Introduction

Microtubules (MTs) are cylindrical polymeric constructs that are 25 nm in diameter and that, in most eukaryotic cells, are a fundamental component of the cell cytoskeleton. They play an essential role in a tremendous number of physiological processes and can self-arrange in vivo into supra-molecular structures such as mitotic spindles. MTs also provide a substrate suitable for the translocation of motor proteins, most of which preferentially move towards one of the two ends of MTs [1]; MTs are thus functionally polarized. As a result of these unique properties, MTs have received consideration for nano-electronics [2, 3], as a template material for metallic nano-structures [4, 5] and as the basis for the development of nano-machines [6, 7]. We also anticipate that MTs will eventually serve as templates for the self-assembly of functional materials and devices in a manner comparable to the way DNA was recently employed [8, 9]. The unique advantage offered by the use of MTs is the multiplicity of the possible interactions that can be exploited on top of the physical interactions and specific bindings that are usually involved in templated self-assembly. MTs can indeed sustain a unique set of interactions mediated by motor proteins (the kinesin and dynein families in particular). Nevertheless, progress towards such MT-templated self-assembly (especially motor-mediated) is hampered by the fact that MTs are prone to damage and denaturation, and that practical nano-transportation critically depends on one's ability to control MT polarity when arranging them on a surface.

Such control over polarity has been reported in the literature by several groups [10–13] while immobilization without functional orientation—a somewhat less demanding challenge—was achieved through several

avenues including covalent binding [14] and specific adsorption [15]. Physical adsorption was also demonstrated for immobilizing MTs onto positively charged surfaces, the later being prepared either by formation of self-assembled monolayers (SAMs) [16, 17] or more simply by adsorption of polymers with a positively charged backbone such as poly-lysine [18, 19]. To the best of our knowledge, variations on the deposition methods based on adsorption have never been thoroughly investigated (although molecular combing was reported in [20]) and neither was capillary-force-assisted MT self-assembly. These methods have proven versatile for creating ordered structures (see for example [21–23]) and their potential for MT self-assembly on surfaces consequently deserves consideration. They are all the more relevant when taking into account the self-organizational properties of MTs in solution [24] that might be preserved during transfer on a substrate.

We thus investigated MT physisorption, self-assembly and combing as a way to create ordered MT templates for further assembly at the nano-scale. We only considered MTs stabilized with the drug Taxol because it is believed to bind onto sites inside the lumen of the MTs [25]. It thus presumably tampers minimally with the functionality of the MT surface. We first adsorbed MTs onto various substrates (highly oriented pyrolytic graphite (HOPG), bare glass, poly-lysine-coated glass, Indium-Tin Oxide (ITO) and metals such as Aluminium, Gold, Chromium) by evaporation of droplets of MT-containing solutions, without preliminary chemical modification of the surfaces. We identified the parameters through which we could control the repeatable self-assembly of structures such as dense films or bundles (dilution method, adsorption time, presence of surfactant). We also probed and achieved molecular combing of MTs through various techniques: blotting and dragging MT solutions on a surface with a filter paper and evaporating solutions under geometrical constraints. The latter approach is similar in concept to the capillarity-driven methods of pattern formation reported recently [26, 27]. We also spin-coated MT solutions in an attempt to use methods previously applied to carbon nanotubes [28], but obtained mixed results in terms of surface coverage and pattern repeatability. The films obtained by the above methods were finally characterized by several imaging techniques, namely: field-emission scanning electron microscopy (FESEM), atomic force microscopy (AFM) and optical microscopy (brightfield, darkfield, fluorescence and polarized light). The approach discussed herein will hopefully facilitate the future development of MT-based technologies (scaffolding and MT-templated self-assembly) as well as MT-based devices (biosensors, nano-machines).

Materials and methods

Preparation of microtubules

The preparation of MTs was carried out essentially as described elsewhere [29], with a few modifications. Tubulin (a mixture of alpha- and beta-monomers) was prepared from four porcine brains by two cycles of temperature-dependent polymerizations and phosphocellulose chromatography. Tubulin concentration was determined by Bradford assay. It was then stored in liquid nitrogen at a concentration of 4 mg · ml^{-1} after appropriate dilution in a buffer with the following composition: 100 mM Piperazine-*N,N'*-bis(2-ethanesulfonic acid) (PIPES) adjusted to pH 6.8 with Sodium hydroxide, 1 mM ethylene glycol-bis(beta-aminoethyl ether)-*N,N,N′N′*-tetra-acetic acid (EGTA), 1 mM magnesium sulfate ($MgSO_4$) and 0.5 mM guanosine 5′-triphosphate sodium salt hydrate (GTP).

Polymerization of tubulin into MTs was induced by thawing a 100 µl aliquot of stock tubulin, then adding 1 mM $MgSO_4$ and 1 mM GTP, then finally heating in a water bath at 37 °C for 30 min. At the end of the polymerization step, the resulting MTs were stabilized by adding Taxol to a final concentration of 40 µM. Fluorescent microtubules were prepared by polymerizing 30 µl of normal tubulin stock solution with $MgSO_4$ and GTP as described above, plus 3 µl of tubulin labeled with rhodamine (5-(and-6)carboxytetramethylrhodamine, Molecular Probes C1171). The resulting solution of fluorescent MTs was kept shielded from light at room temperature and used within 24 h.

For use in experiments, the MT solutions were diluted 1:100 in either distilled water supplemented with 20 µM Taxol, BRB80 buffer (80 mM PIPES, 1 mM $MgCl_2$, 1 mM EGTA) supplemented with 20 µM Taxol, or BRB80 supplemented with 20 µM Taxol and 0.5% Triton × 100 surfactant (this particular buffer will hereafter be referred to as BRB80-TX100).

Even though BRB80 is usually used for dilution in motor assays, distilled water was used to try and circumvent the potential issue of salt co-deposition during the drying of protein solutions, as well as probing the influence of the screening of the surface charges by ions in solution. As MTs are known to depolymerize when exposed to distilled water, we considered that such diluted MT solutions were stable only if used within 5 h of their preparation, although some shortening and a reduction in MT density could be clearly seen to have occurred even after this short period. Moreover, in some experiments unpolymerized tubulin was removed from MT solutions by centrifugation in a table-top centrifuge (Chibitan-R, Millipore) through Ultrafree MC filters (Millipore). Although this approach is interesting insofar as it prevents free tubulin

from competing with MTs for whatever interaction is available to them during experiments, it also introduces a major uncertainty on their final concentration and, as such, was not systematically used.

Preparation of samples

Various substrates were used for deposition of droplet of MT-containing solution. Clean bare glass substrates, both hydrophobic (Matsunami cover glasses Neo 24 × 36 mm) and hydrophilic (Matsunami S7213 glass slides), as well as poly-lysine-coated glass substrates (Matsunami S7111 glass slides) were used without chemical modification. Highly Oriented Pyrolytic Graphite (HOPG, ZYH grade, Veeco Metrology Group) was used freshly cleaved. For investigation of the interaction of the MT solution with electrically conductive substrates, various metals (Aluminium, Gold, Chromium) were evaporated, and Indium-Tin Oxide was sputtered onto cleaned glass cover slides.

All samples were prepared by one of either the following methods: (1) drop drying: a 4-µl drop of solution was deposited onto the sample, placed in a Petri dish and left to dry at room temperature for 24 h on a workbench. (2) blotting and combing: a 2-µl drop of solution was deposited onto the sample and left to settle for one to five minutes, then was blotted with a filter paper. (3) Combing by constrained evaporation: 4 µl of solution were deposited onto the sample substrate and a cover glass (Matsunami Neo, 24 × 18 mm) was placed directly on top of it. Alternatively, a flow cell approximately 100 µm high was constructed as described elsewhere [11] and 12 to 16 µl of solution were injected and left to evaporate. (4) Spin-coating: 50 µl of solution were deposited onto glass slides (with or without poly-lysine) which were subsequently spun for 30 s on a standard spin-coater (Mikasa) at speeds comprised between 300 and 3,000 rpms

Imaging methods

AFM images were obtained in air with a JEOL SPM 4200 used in tapping mode. The cantilever used were from Olympus Co. (OMCL-AC160TS-C2) with a resonant frequency of 300 kHz and a spring constant of 40 $N.m^{-1}$.

Fluorescence images were obtained with an Olympus BX51 microscope fitted with a × 10 lens (Olympus UPlanFLN, N.A. 0.3), a × 50 lens (Olympus MPlanApo, N.A. 0.95), and a × 60 lens (Olympus UPlanFLN, N.A. 0.9) for imaging wet samples under a cover glass. The same set of lenses were used for non-fluorescent (polarized light, brightfield and darfield) imaging. Pictures were taken with a Nikon Coolpix 4500 digital camera, mounted on the top port of the microscope through two adapters (Olympus U-CDMA3 and Nikon Coolpix MCD) providing additional magnification.

Finally, wide-area images of dried drops were obtained with a Keyence VHX digital microscope, and SEM images were taken on a FESEM (JEOL JS-6300F) without any prior contrast-enhancing treatment of the samples.

Results and discussion

Droplet drying

The observed MT self-assembly phenomena were dependant on the deposition methods as well as the substrate employed. The most salient, controlled and reproducible results have been summarized in Table 1 for convenience,

Table 1 Summary of salient results and observations

Deposition method	Substrate used for deposition					
	Hydrophilic surface		Hydrophobic surface		HOPG	
	BRB80	DIW	BRB80	DIW	BRB80	DIW
Blotted and dragged	No SA	No SA	Combing & dendritic bundles	No SA	No SA	MTs, combing and MT supra-assemblies
Constrained	Dendritic bundles	No SA	Dendritic bundles	Dendritic bundles	ND	ND
Droplet drying	Bundles	Bundles & sheaves	Crystalline film	Sheaves	Reticulation (with triton X)	Dense MT films

''ND'' indicates that the experiment was not done, ''No SA'' that no self-assembled structure could be reliably imaged. The other cases are described in detail in the text, where a proper definition of the terms ''*bundles*'' and ''*dendritic bundles*'' can also be found. ''*Hydrophilic surfaces*'' refers to surfaces with a contact angle lesser than 30 degrees. The term ''*Hydrophobic surfaces*'' thus does not necessarily refer to surfaces with a contact angle greater than 90 degrees. It must be noted that HOPG is not included in the ''*Hydrophobic surfaces*'' due to its unique behavior.

and we will now present them in more detail, along with qualitative explanations of the self-assembly processes involved during creation of the films. It must be noted that HOPG is not included in the ''*Hydrophobic surfaces*'' in Table 1 due to the unique results obtained with this substrate. The reader may refer to the supporting information for more comments on structures and films not specifically discussed hereafter.

Self-assembly of fluorescent MT bundles (filamentous structures globally longer and thicker than individual MTs, with a large dispersion in both length and thickness: see Fig. 1) was repeatedly observed in the deposits prepared from MT solutions that were either diluted in BRB80 buffer and drying on hydrophillic surfaces, or drying on hydrophobic glass surfaces and diluted in BRB80 supplemented with the surfactant Triton X (buffer hereafter referred to as BRB80-TX100). In both cases, the droplets were seen to spread over an initial period of several dozen minutes, thus producing flat droplets with large radii (up to half a centimeter and more) and mobile (advancing) contact lines. In the resulting dried deposits, digital microscopy revealed the presence of a crystal-like film, most likely formed from the salts in solution: indeed, the marginal staining by rhodamine suggests that the proportion of depolymerized tubulin in the film is low. Fluorescence microscopy of the latter revealed that it contained many fluorescent MTs, especially on the outer side of the deposit: some MTs apparently retained their individual character, but most had clearly self-organized into bundles of various sizes (Fig. 1a and b). These were under or inside the crystalline film, as revealed by electronic microscopy, brightfield and digital microscopy (Fig. 1d). The fact that some of the MT bundles could be seen by the latter two microscopy techniques underlines the difference in diameter between these and the individual MTs in the initial solution, since without fluorescence, individual MTs can only be visualized with contrast-enhancing techniques such as darkfield and Nomarski.

Bundle self-assembly has already been described ([30, 31]) in MT solutions supplemented with either positively charged species (electrostatic interactions related to charge inversion phenomena) or inert molecules (steric exclusion). Bundle formation in our experiments seems to obey a different mechanism and can partially be explained by

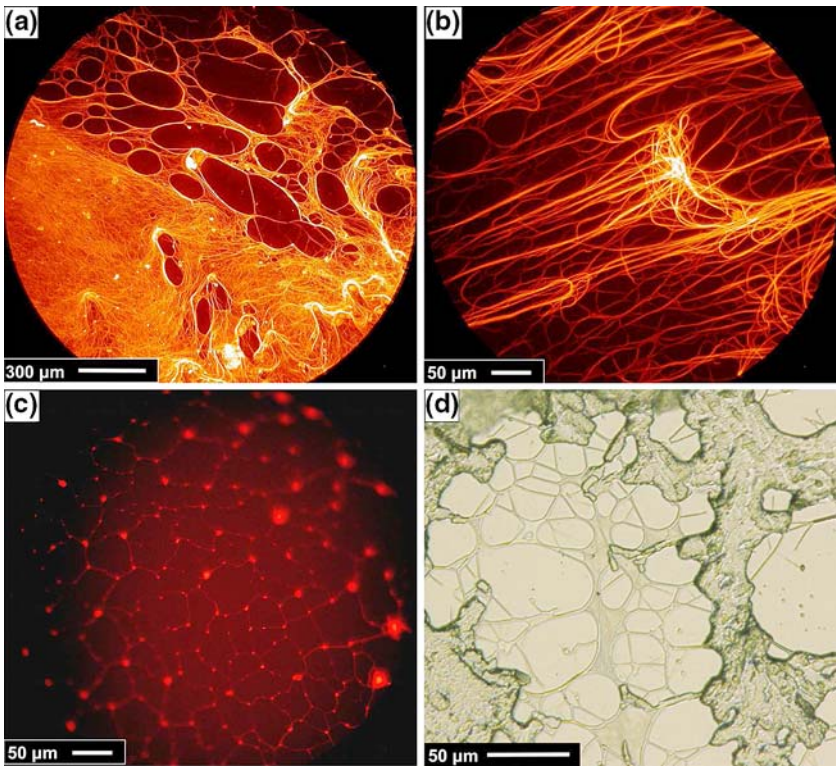

Fig. 1 Formation of MT bundles on various substrates. (**a**–**c**) Fluorescence imaging of microtubules deposited on glass by drying from a MT dilution in BRB80-TX100: (**a**) and (**b**) on glass, (**c**) on HOPG. (**a**) Difference between coronal (bottom left-hand side: fairly homogeneous accumulation of MT bundles) and central area (upper right-hand side: inhomogeneous reticulation of MT bundles) of the deposit. (**b**) MT bundles of various sizes are seen to form entangle. (**c**) Reticulation of the film on HOPG; the coronal area of the image is slightly out of focus due to the local relief of the HOPG surface. (**d**) Image obtained by digital microscopy in the central area of an Aluminium substrate: there, bundles are partially covered by the non-fluorescent film, although in some places the latter also appears *in between* bundles, filling cells of the bundle network

considering the structure of fluid flow inside the drying droplet. Flow lines are indeed present that are mostly attributed to the joint action of contact line pinning and evaporation [32], although other phenomena may also take place under specific experimental conditions [33], such as Marangoni effect or thermal flow. Corresponding zones of dead flow are created where MTs progressively accumulate, especially near the contact line of the drop. There, regardless of whether the contact line is pinned or slowly advancing, MTs agglomerate and form bundles oriented parallel to the contact line, progressively forming a nematic phase where bundles appear. This scenario thus differs from MT bundle formation by condensing agents previously studied [34] and is actually more similar to recent observations of DNA bundle formation in dried droplets [35]. The precise nature of the interaction between MTs inside a bundle is unclear, although electrostatic attraction between rodlike, like-charged polyelectrolytes has been extensively studied both theoretically and experimentally (see for example [36]). The observation of the organization of Mg counterions around and between individual MTs will undoubtedly provide valuable insights into the mechanism of bundle formation, in a manner similar to the reported results on F-actin [37]. The exact composition and inner structure of the bundles, as well as the fate of individual MTs once they become part of them, is also still to be investigated. In particular, an important question from a technological point of view is whether these bundles can still provide physiological functions associated with MTs, such as supporting the movement of motor proteins.

As for the film that covered the self-assembled bundles, we repeatedly observed across most samples a difference in nature between a coronal area on the outside of the drop (homogeneous film) and the central area of the deposit (strongly reticulated film). This difference can be seen clearly in Fig. 1a) and can be explained by the dewetting properties of the solutions. This hypothesis is in good agreement with the results presented by [38] and is supported by the difference in reticulation patterns observed on different substrates (Fig. 1a, c and d): with dilutions in BRB80-TX100 on HOPG, in particular, the edges of the bundle network were thinner and more homogeneous in size than on other surfaces (Fig. 1c). Contrary to the reticulation, however, the difference between the central and outer area of the dried films is a phenomenon that is of a very general nature and is mostly due to two phenomena: (1) the omnipresence of the outward capillary flow, and (2) the formation of a solid crust due to salt crystallization, the presence of which has been shown to influence the final shape of the dried deposit [39].

Taken together, these observations indicate that the differences existing between the final deposits depend mainly on 3 factors: (1) the contact angle of the droplet with the substrates; (2) the pinning (or lack thereof) of the contact line; (3) the physico-chemical properties of the solutions per se. The contact angle is the main parameter controlling the radius of the drying droplet. It thus determines its evaporation dynamics, the distribution of the species in solution and the local solute concentrations reached during evaporation. For example, droplets of MT solutions diluted in BRB80 drying on hydrophobic surfaces had a pinned contact line and a high contact angle: thus they had a smaller radius and produced very specific deposits, characterized by the presence of a thick film. Interestingly, polarized light microscopy revealed the existence of wide-area domains (see Fig. S1 in supporting information) that could individually be brought to extinction by rotation of the sample relative to the crossed polarizers. This is indicative of long-range structural ordering inside the film that can be attributed to both the existence of a MT nematic phase and/or the crystallization of the salts from the buffer. This likely indicates that critical concentrations for crystal growth were reached during evaporation, and one may even hypothesize that MTs possess the ability to modulate the growth of inorganic crystals, as is the case for other proteins [40, 41].

The one remarkable exception to the patterns of droplet drying described above was obtained with HOPG: on this substrate, when using fluorescent MTs diluted in water, films of densely packed MTs self-assembled upon drying inside which individual MTs could be resolved by AFM (Fig. 2). The AFM pictures clearly show the self-organization of the MTs inside the film: they form 2-dimensional rafts of one or two dozens of MTs that together provide a very uniform cover of the surface. MTs do not form bundles, as seen from the width (about 120 nm) of the filamentous structures imaged by AFM (Fig. 2b, d). Taking into account the convolution with the shape of the AFM tip, this measured value is in accordance with previously reported diameters for dried MTs measured by AFM, even though it is well above the theoretical 25 nm diameter of free MTs. We purposefully damaged these films by running the AFM tip across the surface while maintaining contact (Fig. 2c). By measuring the profiles of the resulting scratches (Fig. 2e), we determined the thickness of this film to be around 11 nm, which corresponds to a single layer of adsorbed MTs [18, 17]. The details of the mechanism through which such homogeneous films form at the surface of HOPG are unclear. In particular, non-fluorescent MTs seem to behave differently from fluorescently-labeled ones in terms of self-assembly on HOPG. It may be that the combination of the presence of the label and the low ionic density of the solution favors electrostatic interactions, leading to this particular type of self-assembly (it has to be noted, however, that no similar self-assembly was observed on other conductive substrates such as Aluminium, Chro-

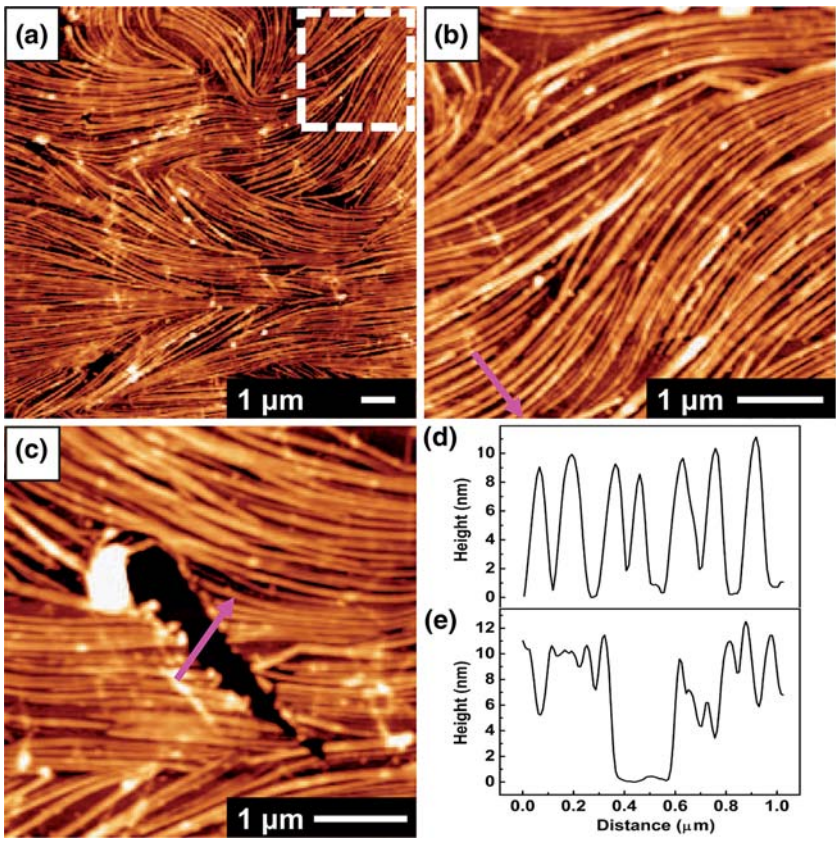

Fig. 2 AFM topographs of microtubules deposited on HOPG by drying from a MT dilution in water. (**a**) self-assembly of dense MT films forming a continuous coverage of the HOPG surface. (**b**) Zoom on the upper right-hand corner of picture (**a**). (**c**) Intentional damage applied to the MT film through the AFM tip. (**d**) AFM profile of the MT film as indicated by the arrow in (**b**). (**e**) AFM profile of the scratch indicated by the arrow in (**c**): the measured depth is around 11 nm, which shows that the film is a monolayer

mium, Gold and ITO). If this is indeed the case, the ability to polymerize MTs from various types of modified tubulin may provide an elegant way to control template formation. In any case, the dense films that were produced on HOPG show great promise for biosensor applications where electrochemical methods are to be used.

Combing by blotting and evaporation under geometrical constraints

Very different self-assembled structures were obtained by blotting MT solutions diluted in BRB80 or letting them evaporate under geometrical constraints. These techniques unequivocally demonstrated the ability to comb MTs and MT bundles on a substrate. Evaporation of MT solutions diluted in BRB80 inside flow cells, in particular, reliably produced large-area patterns of aligned dendritic structures (Fig. 3a) that were reminiscent of reported constructs obtained from DNA [42, 43]. With this technique, we demonstrated self-assembly of dendritic bundles of MTs during the drying process, as depicted in Fig. 3f: some MTs were indeed pinned onto the substrate, probably by a defect of the surface that ''recruited'' other MTs from the solution to form an agglomerate; these were subsequently elongated by the slowly receding contact line, locally deforming the latter in the process before passing through it and finally being left behind (Fig. 3b, c). The branching structure of these bundles is correlated to the direction of the movement of the receding contact line: due to capillary interactions resulting from the deformation of the contact line, adjacent bundles indeed tend to aggregate if they are sufficiently close, forming the observed dendritic structures (Fig. 3f). The latter thus form before the main trunk of the bundle, which is on average longer than the branching dendrites.

AFM imaging revealed a height of 10 to 15 nm for these particular bundles, but it was not possible to investigate further their inner structure. How much of the MTs are actually left inside is thus an open question, as well as the possible polymerization of tubulin into exotic structures. Although the parallel arrangement of MT bundles was the overwhelmingly dominant pattern, individual MTs were also found to be combed on the surface, albeit in smaller patches. Even then, they were often seen to make contact with or twist around one another (Fig. 3e). For producing combed individual MTs, blotting and dragging produced better results, problably because the contact line receded faster. Spin-coating at high speeds (2,000–3,000 rpms) actually also produced interesting results, even though the resulting combing patterns were difficult to reproduce and strongly inhomogeneous across the surface (see Fig. S2 in supporting information). Finally, observation of the films

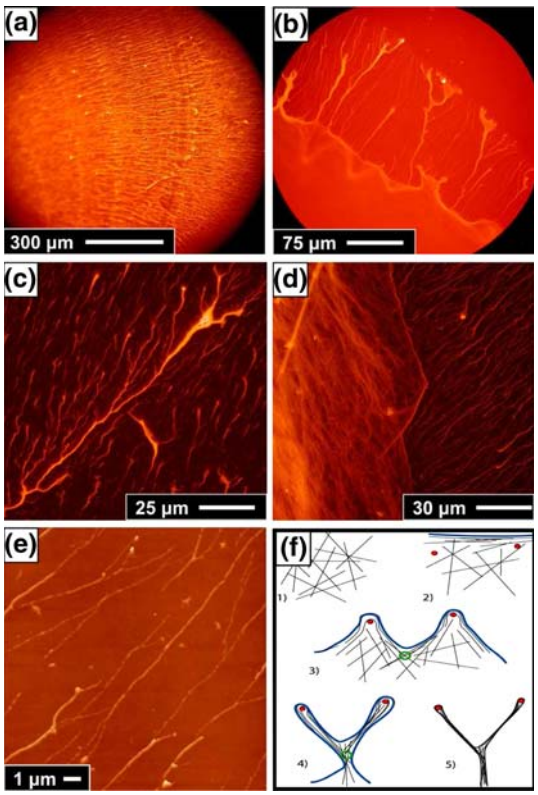

Fig. 3 Formation of dendritic MT bundles by receding contact line. (**a**–**d**) Fluorescent imaging of MT structures self-assembled on glass from a MT solution prepared by dilution in BRB80. Pictures (**b**) (taken during the evaporation of a droplet) and (**d**) (taken at the border of the cover of a flow cell after drying) show the concurrent formation of dendritic and non-dendritic bundles. Non-dendritic bundles are oriented roughly perpendicular to the dendritic ones. In picture (**b**), they also bend periodically due to compressive stress. (**e**) AFM imaging shows combing of individual microtubules after blotting. (**f**) Formation mechanism of the dendritic bundles: (1) MTs randomly float in solution. (2) The contact line (blue) recedes, along which MTs accumulate and orientate. (3) MTs are pinned on defects of the surface (red dots) and induce the deformation of the receding contact line. An MT entanglement area appears (green circle). (4) MTs self-arrange into dendrites under the action of capillary forces. (5) The contact line breaks free from the deposited MTs and continues its recession

obtained at the edges of flow cells showed both the bundles left behind by the receding contact line (and thus combed perpendicularly to it) and those aligned in the dead zone of the outward capillary flow (Fig. 3d). Considering the orientation of the dendritic structure of the combed bundles thus suggests the initial formation of a solid crust at the air-liquid interface: the latter immobilized the bundles aligned in the dead flow areas before the contact line started receding. These observations thus underline the fundamental influence of contact line pinning on the final structure and orientation of the deposited microtubules.

Finally, we observed peculiar patterns of self-assembly on samples prepared on HOPG by blotting MT solutions diluted in water. Several large crystals were indeed observed, with regions between them rich in films containing MTs that could readily be imaged by AFM (see Fig. S3 in supporting information). These MTs formed multi-layer films and exhibited a surprisingly rich repertoire of patterns of organization: in some areas, MTs were arranged densely but randomly (Fig. 4a, c), forming an incomplete, discontinuous layer on the surface, on top of which different self-assembled structures could be seen (Fig. 4a, b). In other areas, the MT density was markedly lesser and some individual MTs were locally combed. The combing effect did not follow the HOPG steps (Fig. 4d), contrary to what happens in some specific cases with DNA [44]. Moreover, in all many cases we observed that some MTs would ''stick together'' along their main axis, which was likely caused by capillary forces during drying. The same explanation could account for the observation of large bundle structures (Fig. 4a) of various sizes, seemingly stiffer than individual MTs as denoted by their rectitude over several micrometers (Fig. 4b, c). The structure of these bundles is unclear. In particular, the existence and nature of some form of ligand between the individual tubular structures inside the bundles is an open question. Considering the sheaves formed in water by Taxol (see Fig. S4 in supporting information), its role in the formation of such large bundles should also be investigated. Another salient feature of the AFM images is that many MTs were observed to disappear under a film left behind during blotting (Fig. 4e). The latter is likely composed of salt crystals, even though, given the dilution in water, it may also comprise depolymerized tubulin. Interestingly, this film seems to have occasionally been pinned during drying by the individual MTs, (this is clearly highlighted in Fig. 4f), thus showing that those MTs perpendicular to the contact line of the receding liquid have a better chance to remain free on the surface after drying.

Summary and perspectives

In the present work, we studied the physisorption of Taxol-stabilized MTs as a step towards MT-templated self-assembly. We probed the influence of the nature of the substrate, of the dilution methods and of the deposition protocols on the resulting adsorbed films. We thus successfully produced dense films of self-assembled MTs on HOPG by drying droplets of water-diluted MT solutions. Auto-assembled, non-dendritic bundles were also produced by solvent evaporation on surfaces having a low contact angle with the drying solution, a state that could be attained by addition of a surfactant (Triton X 100) when necessary. This method differs from those previously reported in the literature, based on either charge inversion or steric

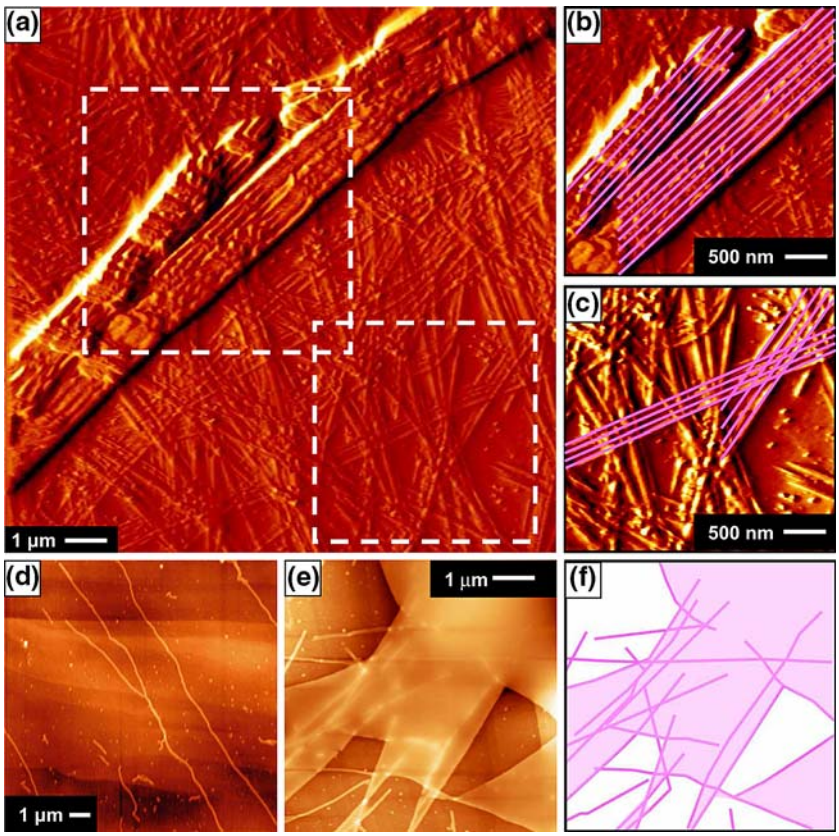

Fig. 4 AFM imaging of MTs arranged on HOPG by blotting and dragging. (**a**–**c**) Large supra-molecular assembly of MTs laying on top of a network of entangled individual MTs. (**b**) Close-up of the supra-molecular structure depicted in a); the MTs comprising the supra-molecular structure are straightened. (**c**) Close-up of the entangled MT network depicted in (**a**); grouping and straightening is also observed within this network, albeit involving fewer MTs. (**d**) Individual MTs laid across steps (horizontal stripes) in HOPG. (**e**–**f**) Individual MTs disappearing under a film; as highlighted in (**f**), the film has formed between some MTs, probably as a result of liquid pinning by these MTs during the drying process

exclusion. Finally, self-assembly of MT dendritic bundles was achieved by evaporation under geometrical constraints such as a flow cell. The electronic, optical and biological properties of the various bundles described in the present work will be interesting to study as they may be used in the future beyond their intended role as templates for self-assembly of functional materials.

Our observations of droplet evaporation show that the interplay between MT self-organization, interactions with the surface and capillary flow controls the final shape, structure and homogeneity of the final dried deposit. The implication of these observations is that production of spotted arrays of MTs on glass or silicon substrates (similar to DNA arrays) must take into account the evaporation dynamics of the spotted droplets, and that strategies must be developed so as to obtain MTs that are both functional and free from any film above them.

Moreover, the combing of both individual MTs and MT bundles that was achieved when using MT solutions dried in flow cells or blotted and dragged across a surface opens intriguing possibilities. The directionality of the structures produced by these methods could be of particular interest for nano-transportation systems provided the combed structures exhibit at least some of the physiological functions associated with individual MTs. This point is of crucial importance and is still under investigation. If the combed structures still support translocation of motor proteins, the combing techniques described in the present work will have important practical applications for both the development of both nano-machines and MT-templated self-assembly technology.

Finally, the results presented here also point at a strong specific interaction between HOPG surface and MTs in solution with low ionic strength. Although the nature of this interaction is not fully understood, it could be exploited to reliably produce dense and homogeneous films of adsorbed MTs. This, coupled with the ability to fabricate devices integrating HOPG micro-electrodes [45], may pave the way to the development of electrochemical sensors integrating MTs. One may thus envision designing assays based on this technology to quantify the interactions of proteins and molecules with MTs, which, given MT implication in heavy pathologies (cancer, Alzheimer's), represents a considerable—and, as yet, unexplored—opportunity for pharmaceutical research.

Acknowledgments F.O.M. and F.R. acknowledge the financial support of the Japan Society for the Promotion of Science (JSPS). P.M. acknowledges the financial support of the Centre National de la Recherche Scientifique (CNRS). F.O.M. and M.C.T. acknowledge prof. S. Takeuchi for permitting the use of ultra-centrifuges.

References

1. N. Hirokawa, R. Takemura, Nature Rev. Neurosc. **6**, 201–214 (1995)
2. W. Fritzsche, J.M. Köhler, K.J. Böhm, E. Unger, T Wagner, R. Kirsch, M. Mertig, W. Pompe, Nanotechnology **10**, 331–335 (1999)
3. W. Fritzsche, K.J. Böhm, E. Unger, J.M. Köhler, Appl. Phys. Lett. **75**, 2854–2856 (1999)
4. S. Behrens, K. Rahn, W. Habicht, K.J. Böhm, H. Rösner, E. Dinjus, E. Unger, Advanced Mat. **14**, 1621–1625 (2002)
5. S. Behrens, W. Habicht, J. Wu, E. Unger, Surf. Interf. Anal **38**, 1014–1018 (2006)
6. L. Jia, S.G. Moorjani, T.N. Jackson, W.O. Hancock, Biomed. Microdev. **6**, 67–74 (2004)
7. H. Hess, G.D. Bachand, V. Vogel, Chem. Eur. J. **10**, 2110–2116 (2004)
8. H. Yan, S.H. Park, G. Finkelstein, J.H. Reif, T.H LaBean, Science **301**, 1882–1884 (2003)
9. J. Zheng, P.E. Constantinou, C. Micheel, A.P. Alivisatos, R.A. Kiehl, N.C. Seeman, Nano Lett. **6**, 1502–1504 (2006)
10. R. Stracke, J. Burghold, H.J. Schacht, K.J. Böhm, E. Unger, Nanotechnology **11**, 52–56 (2000)
11. R. Yokokawa, S. Takeuchi, T. Kon, M. Nishiura, K. Sutoh, H Fujita, Nano Lett. **4**, 2265–2270 (2004)
12. L. Limberis, J.J. Magda, R.J. Stewart, Nano Lett. **1**, 277–280 (2001)
13. Y. Yang, P.A. Deymier, L. Wang, R. Guzman, J.B. Hoying, H.J. McLaughlin, S.D. Smith, I.N. Jongewaard, Biotech. Progress **22**, 303–312 (2006)
14. W. Roos, J. Ulmer, S. Gräter, T. Surrey, J.P. Spatz, Nano Lett. **5**, 2630–2634 (2005)
15. G. Muthukrishnan, C.A. Roberts, Y.-C. Chen, J.D. Zahn, W.O. Hancock, Nano Lett. **4**, 2127–2132 (2004)
16. A. Vinckier, I. Heyvaert, A. D'Hoore, T. McKittrick, C.V. Haesendonck, Y. Engelborghs, L. Hellemans, Ultramicroscopy **57**, 337–343 (1995)
17. P.J. de Pablo, I.A.T. Schaap, C.F. Schmidt, Nanotechnology **14**, 143–146 (2003)
18. W. Vater, W. Fritzsche, A. Schaper, K.J. Böhm, E. Unger, T.M. Jovin, J. Cell Sc. **108**, 1063–1069 (1995)
19. Y. Yang, R. Guzman, P.A. Deymier, M. Umnov, J. Hoying, S Raghavan, O. Palusinski, B.J.J. Zelinski, J. Nanosc. Nanotech. **5**, 2050–2056 (2005)
20. W. Fritzsche, K.J. Böhm, E. Unger, J.M. Köhler, Nanotechnology **9**, 177–183 (1998)
21. M. Maillard, L. Motte, M.-P. Pileni, Advanced Mat. **13**, 200–204 (2001)
22. E. Rabani, D.R. Reichman, P.L. Geissler, L.E. Brus, Nature **426**, 271–274 (2003)
23. M.A. Ray, H. Kim, L. Jia, Langmuir **21**, 4786–4789 (2005)
24. J. Tabony, N. Glade, J. Demongeot, C. Papaseit, Langmuir **18**, 7196–7207 (2002)
25. E. Nogales, M. Whittaker, R.A. Milligan K.H. Downing, Cell **96**, 79–88 (1999)
26. Z. Lin, S. Granick, J. Am. Chem. Soc. **127**, 2816–2817 (2005)
27. S.W. Hong, J. Xu, J. Xia, Z. Lin, F. Qiu, Y. Yang, Chem. Mat. **17**, 6223–6226 (2005)
28. A.B. Dalton, A. Ortiz-Acevedo, V. Zorbas, E. Brunner, W.M. Sampson, S. Collins, J.M. Razal, M. Miki Yoshida, R.H. Baughman, R.K. Draper, I.H. Musselman, M. Jose-Yacaman, G.R. Dieckmann, Adv. Funct. Mat. **14**, 1147–1151 (2004)
29. R. Yokokawa, Y. Yoshida, S. Takeuchi, T. Kon, H. Fujita, Nanotechnology **17**, 289–294 (2006)
30. J.X. Tang, S. Wong, P.T. Tran, P.A. Janmey, Ber Bunsenges. Phys. Chem. **100**, 796–806 (1996)
31. J.X. Tang, T. Ito, T. Tao, P. Straub, P.A. Janmey, Biochemistry **36**, 12600–12607 (1997)
32. R.D. Deegan, O. Bakajin, T.F. Dupont, G. Huber, S.R. Nagel, T.A. Witten, Nature **389**, 827–829 (1997)
33. Y.Y. Tarasevich, Phys. Uspekhi **47**, 717–728 (2004)
34. D.J. Needleman, M.A. Ojeda-Lopez, U. Raviv, K. Ewert,; H.P. Miller, L. Wilson, C.R. Safinya, Proc. Nat. Acad. Sc. USA **101**, 16099–16103 (2004)
35. I.I. Smalyukh, O.V. Zribi, J.C. Butler, O.D. Lavrentovich, G.C.L. Wong, Phys. Rev. Lett. **96**, 177801 (2006)
36. O.V. Zribi, H. Kyung, R. Golestanian, T.B. Liverpool, G.C.L. Wong, Phys. Rev. E **73**, 031911 (2006)
37. T.E. Angelini, H. Liang, W. Wriggers, G.C.L. Wong, Eur. Phys. J. E **16**, 389–400 (2005)
38. L.W. Schwartz, R.V. Roy, R.R. Eley, S. Petrashy, J. Coll. Interf. Sc. **234**, 363–374 (2001)
39. T. Kajiya, E. Nishitani, T. Yamaue, M. Doi, Phys. Rev. E **73**, 011601 (2006)
40. K. Shiba, T. Honma, T. Minamisawa, K. Nishiguchi, T. Noda, EMBO Reports **4**, 148–153 (2003)
41. B. Szabó, T. Vicsek, Phys. Rev. E **67**, 011908 (2003)
42. G. Maubach, W. Fritzsche, Nano Lett. **4**, 607–611 (2004)
43. T. Heim, S. Preuss, B. Gerstmayer, A. Bosio, R. Blossey, J. Phys. Cond. Matt. **17**, S703–S716 (2005)
44. F. Rose, P. Martin, H. Fujita, H. Kawakatsu, Nanotechnology **17**, 3325–3332 (2006)
45. A.M. Oliveira Brett, DNA-based biosensors. In: *Biosensors and Modern Biospecific Analytical Techniques*, Volume XLIV (Comprehensive Analytical Chemistry), ed. by L. Gorton, (Elsevier Science: Amsterdam, 2005)